J. Fluid Mech. (1986), *vol.* 168, *pp.* 479–500
Printed in Great Britain

The generation of capillary instabilities on a liquid jet

By S. J. LEIB AND M. E. GOLDSTEIN
NASA Lewis Research Center, Cleveland, OH 44135, USA

(Received 7 October 1985)

The coupling between imposed disturbances and capillary instabilities on a liquid jet is examined. It is shown that in most physical situations the forcing produces neutral waves which can then turn into growing waves as the profile relaxes or may be amplified nonlinearly by a mechanism of the type considered by Akylas & Benney (1980). The effectiveness of the coupling is expressed quantitatively by numerically computed values of the 'coupling coefficient'.

1. Introduction

It is now believed that the breakup of liquid jets into drops begins with the excitation of Rayleigh or capillary instabilities by weak external disturbances. This phenomenon was first studied mathematically (Rayleigh 1878, and others) by treating the jet as a doubly infinite parallel flow and determining when that flow becomes unstable to temporally growing instability waves. But it was natural for the experimentalists to approach this problem by imposing controlled harmonic (usually acoustic) disturbances of a single frequency, say ω, on their flows (either from within or from outside their nozzles) which then generate spatially amplifying waves that are closely related to the temporally growing instability waves of Rayleigh (1878). There are also a number of technological devices, the ink-jet printer and the liquid droplet radiator, for example, that rely on the excitation of spatially amplifying Rayleigh waves to produce controlled breakup of liquid jets. Keller, Rubinow & Tu (1973) analysed the spatially amplifying capillary waves by transforming Rayleigh's (1878) dispersion relation to a moving jet and keeping the frequency real while allowing the wavenumber to be complex. They found that the temporal and spatial growth rates only agree in the infinite Weber number limit (where the Weber number is defined to be $(\rho a/\gamma)\, U_0^2$, ρ and γ being the density and surface tension, and a and U_0 being a characteristic length and velocity). The primary purpose of this paper is to understand how these instability waves are generated by the externally imposed disturbances, or in Morkovin's (1969) words, to analyse the 'receptivity' of the flow. Our main interest is in the technologically (and experimentally) important case where the wavelength of the imposed disturbance is very long (effectively infinite) compared to the wavelength of the Rayleigh instability. The wavelength matching then relies on the 'scattering' of the imposed disturbance at the nozzle lip, and it is therefore necessary to study the semi-infinite jet/semi-infinite nozzle configuration shown in figure 1 rather than the doubly infinite jet analysed by Rayleigh (1878), Keller *et al.* (1973), etc. We shall suppose that the flow is excited from within the nozzle and take the incident disturbance to be a uniform pulsation of the entire flow, corresponding to a plane acoustic wave in the zero-Mach-number limit to which the analysis is confined.

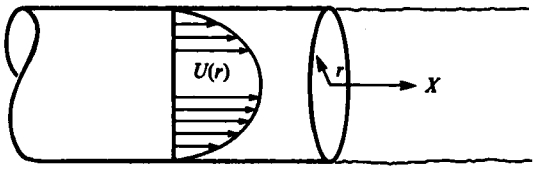

FIGURE 1. Flow geometry.

Similar problems were analysed by Crighton & Leppington (1974) for the Kelvin–Helmholtz instability on the vortex sheet behind a semi-infinite flat plate (with zero velocity on one side) and by Munt (1977), Rienstra (1981) and Cargill (1979) for the Kelvin–Helmholtz instability on a plug-flow jet emanating from a round nozzle.

In the present case, it is more appropriate to assume that the mean flow has a Hagen–Poiseuille or parabolic profile rather than the plug-flow profile analysed by Munt (1977), Rienstra (1981), Cargill (1979), Rayleigh (1878) and Keller *et al.* (1973). It turns out that the Rayleigh equation, which governs the unsteady motion within the flow, is the same for this profile as it is for the plug flow, so that the problem can be solved just as easily for the former profile as for the latter. In fact, the same Rayleigh equation applies to a more general parabolic profile that involves arbitrary velocity slip at the wall.

The mean flow can be treated as independent of the streamwise coordinate for purposes of analysing the receptivity problem, i.e. for purposes of determining the 'coupling coefficient', which relates the initial amplitude of the instability wave to that of the imposed disturbance, and the most appropriate profile to use in the analysis is the Hagen–Poiseuille profile. But it turns out that the spatially growing Rayleigh instability waves only exist on this profile for very small Weber numbers, and then only for Strouhal numbers ($\omega a/U_0$) below a very low 'cutoff' value. Outside of this range they are replaced by a neutral (i.e. non-growing) disturbance that propagates downstream from the nozzle lip. But the range of unstable Weber and Strouhal numbers increases enormously as the mean flow gradually relaxes to a plug-flow profile far downstream from the nozzle exit. It is therefore necessary to calculate the gradual development of the instability wave from the initially neutral disturbance in order to determine the final amplitude of that wave. We do this by using the 'slowly varying approximation', which assumes that the local growth rate can be calculated by using the local mean flow profile while neglecting variations in the streamwise direction. The required local profiles are well described by the generalized Hagen–Poiseuille profiles alluded to above. We therefore analyse the instability wave for this general class of profiles but evaluate the coupling coefficient only for the Hagen–Poiseuille profile and (for purposes of comparison) the plug-flow profile.

Since it is not *a priori* possible to distinguish between amplifying disturbances and evanescent waves, we cannot impose enough boundary conditions at infinity to uniquely determine the steady-state solution to the present problem. This will occur for any problem involving an 'active system' that can support amplifying waves (Briggs 1964) and is usually dealt with by treating the steady-state solution as the long time limit of the 'causal' solution to the appropriate initial-value problem. This was, in fact, done by Crighton & Leppington (1974), Munt (1977) and Cargill (1979) for the related problems (alluded to above) involving Kelvin–Helmholtz waves. They showed that there were infinitely many causal solutions, but only one that was non-singular at the trailing edge. The present situation is somewhat different, in that

the non-singular causal solution is the only solution that exists as an ordinary function. The 'more singular solutions' would have to be interpreted in the sense of distributions and would then involve delta function-type singularities at the edge. It seems to us that such solutions are easily dismissed on physical grounds.

Far downstream in the flow the unsteady motion is described by an unimportant fluctuation in the overall pressure level and either the spatially amplifying Rayleigh wave for Strouhal numbers below cutoff or one or two neutral disturbances (one of which turns into the Rayleigh wave in the unstable range of Weber and Strouhal numbers) for Strouhal numbers above cutoff. It is interesting to note that there is a certain range of parameters where the neutral Rayleigh wave has upstream group velocity even though it appears downstream of its source (i.e. the trailing edge). Similar behaviour was found by Brazier-Smith & Scott (1984) but they were able to dismiss it as asymptotically insignificant (in the Poincaré sense) since it always occurred in the presence of an amplifying disturbance which would dominate the negative group velocity wave.

Steady-state analysis of flows (such as the one under consideration) that support amplifying waves only makes sense if imposed disturbances do not exhibit unlimited growth in time at any fixed point in space, that is, if the system is not 'absolutely unstable'. It is shown below that the present flow is 'absolutely unstable' for Weber numbers below a certain critical value which increases as the profile approaches a plug flow.

The dispersion relation is found to have double roots at certain real frequencies. The consequences of such double roots were discussed for the case of real wave numbers (and complex or real frequencies) by Akylas & Benney (1980). They referred to it as 'direct resonance' and showed that it can cause a significant change in the behaviour of the temporally growing weakly nonlinear instability waves. The implications of this phenomenon for the present time harmonic solution are discussed in §5.

The receptivity problem is formulated in §2. It is then solved using the Wiener–Hopf method. The dispersion relation for the generalized Hagen–Poiseuille velocity profile is analysed in §3. To our knowledge, this is the first analysis of the capillary instability of the Hagen–Poiseuille profile, not to mention the generalized profile. A discussion of the coupling coefficient, the validity of the locally parallel flow assumption and other results are presented in §4.

2. Analysis

2.1. *Formulation*

We consider an inviscid incompressible flow of a liquid of density ρ and surface tension γ, emerging from a semi-infinite duct of radius a into an evacuated region, as shown in figure 1. We suppose that a steady base flow, which we initially assume to be parallel with velocity profile $U(r)$, is subjected to a small amplitude uniform axial velocity fluctuation,

$$u_\infty \, \mathrm{e}^{-\mathrm{i}\Omega t},$$

far upstream within the nozzle. Here, r denotes the radial coordinate, which we assume along with all other lengths to be normalized by a, t denotes the time normalized by $a/\bar{U}$, where $\bar{U}$ is the mass-averaged mean velocity, Ω denotes the Strouhal number based on $\bar{U}$ and a, and we assume that U has been normalized by $\bar{U}$ so that

$$2\int_0^1 rU(r)\,\mathrm{d}r = 1. \tag{2.1}$$

Since the resulting unsteady motion will be axisymmetric, it can be expressed in terms of a stream function ψ such that

$$u = \frac{1}{r}\frac{\partial \psi}{\partial r}; \quad v = -\frac{1}{r}\frac{\partial \psi}{\partial x}, \tag{2.2}$$

where u and v denote the axial and radial velocity fluctuations normalized by u_∞, and x denotes the normalized streamwise coordinate.

It is convenient to introduce the function ϕ by

$$\phi_x = \psi, \tag{2.3}$$

and it then follows from the linearized streamwise momentum equation that p, the pressure fluctuation normalized by $\rho \bar{U} u_\infty$, is given by

$$-rp = \left(\frac{\partial}{\partial t} + U\frac{\partial}{\partial x}\right)\phi_r - U'\phi_x, \tag{2.4}$$

where the prime denotes differentiation with respect to r. ϕ is determined by the linearized vorticity equation (or Rayleigh equation)

$$\left(\frac{\partial}{\partial t} + U\frac{\partial}{\partial x}\right)\left(\nabla^2 - \frac{1}{r^2}\right)\left(\frac{\phi}{r}\right) - \left(\frac{U'}{r}\right)'\phi_x = 0, \tag{2.5}$$

where

$$\nabla^2 = \frac{1}{r}\frac{\partial}{\partial r} r \frac{\partial}{\partial r} + \frac{\partial^2}{\partial x^2}, \tag{2.6}$$

is the Laplacian, subject to the boundary conditions of no flow through the walls in the duct region

$$v = 0; \quad -\infty < x < 0, \tag{2.7}$$

and the kinematic and dynamic boundary conditions

$$\left.\begin{aligned} v &= \left(\frac{\partial}{\partial t} + U\frac{\partial}{\partial x}\right)\zeta \quad 0 < x < \infty \\ \text{and} \qquad p &= -\frac{1}{\beta}(\zeta + \zeta_{xx}) \end{aligned}\right\} \tag{2.8}$$

respectively, in the jet region at $r = 1$, where $\beta \equiv \rho a \bar{U}^2/\gamma$ is the Weber number and ζ is the displacement of the jet surface relative to its undisturbed position (Drazin & Reid 1981, pp. 22–24).

Since the problem is linear and we are interested only in the steady-state solution, ϕ will have harmonic time dependence, and it is convenient to write ϕ as the sum of the solution for the forced flow in a doubly infinite duct and an unknown function $\phi^{(1)}$ which accounts for the free surface, as

$$\phi = \left[\frac{r^2}{2}\left(x - \frac{P_0}{i\Omega}\right) - \frac{r^2 U - 4\int r U \, dr}{2i\Omega} + \phi^{(1)}(r, x)\right] e^{-i\Omega t}, \tag{2.9}$$

where P_0 is an arbitrary constant that sets the overall level of the pressure fluctuation in the duct. Then $\phi^{(1)} e^{-i\Omega t}$ satisfies (2.5) and it follows from (2.2)–(2.4), and (2.7)–(2.9) that

$$\left.\begin{aligned} \phi^{(1)}_{xx} &= 0 \quad \text{for } x < 0, \quad r = 1 \\ -\phi^{(1)}_{xx} &= -i\Omega\zeta + U\zeta_x \quad \text{for } x > 0, \quad r = 1 \end{aligned}\right\}, \tag{2.10}$$

$$\theta^{(1)} - U'\phi^{(1)}_x - \frac{1}{\beta}(\zeta + \zeta_{xx}) = i\Omega x - P_0 \quad \text{for } x > 0, \quad r = 1, \tag{2.11}$$

and
$$\phi^{(1)}_{xr} \to 0 \quad \text{as } x \to -\infty,\ 0 \leqslant r \leqslant 1, \tag{2.12}$$

where
$$\theta^{(1)} \equiv \left(-\mathrm{i}\Omega + U\frac{\partial}{\partial x}\right)\phi^{(1)}_r. \tag{2.13}$$

We consider the one-parameter family of mean velocity profiles

$$U(r) = \frac{1-br^2}{1-\frac{1}{2}b}, \tag{2.14}$$

which produces progressively flatter profiles as the parameter b goes from 1 (Hagen–Poiseuille profile) to zero (plug profile) and hence will serve to model the profile relaxation referred to in §1. It follows from (2.5) and (2.9) that $\phi^{(1)}/r$ satisfies

$$\left(\nabla^2 - \frac{1}{r^2}\right)\left(\frac{\phi^{(1)}}{r}\right) = 0, \tag{2.15}$$

independently of b.

As indicated in §1, we are interested in obtaining the steady-state causal solution to (2.10)–(2.15). We do this by using Briggs' (1964) method, which requires that we allow Ω to have an arbitrarily large positive imaginary part and find the real Ω solution by analytic continuation. We construct the relevant complex Ω solution by using the Wiener–Hopf technique (Noble 1958 p. 36).

2.2. *Solution*

We introduce the half-range transforms

$$\hat{\phi}_{\mp}(k,r) = \pm\frac{1}{2\pi}\int_0^{\pm\infty} \phi^{(1)}(x,r)\,\mathrm{e}^{-\mathrm{i}kx}\,\mathrm{d}x, \tag{2.16}$$

where the upper and lower signs go together and $\hat{\phi}_+$ ($\hat{\phi}_-$) is an analytic function in the upper (lower) half of the complex k-plane (Roos 1969 p. 114). Then,

$$\hat{\phi} \equiv \hat{\phi}_+ + \hat{\phi}_-, \tag{2.17}$$

is the usual (full range) Fourier transform and the boundary-value problem equations (2.10)–(2.15) become, upon noting that $\zeta(0) = 0$,

$$\hat{\phi}_+ = 0, \tag{2.18}$$

$$k^2\hat{\phi}_- = -\mathrm{i}\left(\Omega - \frac{1-b}{1-\frac{1}{2}b}\,k\right)\hat{\zeta}_-, \tag{2.19}$$

$$-\hat{\theta}_- - \frac{2b\mathrm{i}}{1-\frac{1}{2}b}\,k\hat{\phi}_- - \frac{k^2-1}{\beta}\,\hat{\zeta}_- = \frac{1}{2\pi\beta}\,\zeta_x(0) + \frac{\mathrm{i}\Omega}{2\pi(k-\mathrm{i}\epsilon^*)^2} - \frac{\mathrm{i}P_0}{2\pi(k-\mathrm{i}\epsilon^*)}, \tag{2.20}$$

for $r = 1$, and
$$r\left(\frac{1}{r}\,\hat{\phi}'\right)' - k^2\hat{\phi} = 0, \tag{2.21}$$

for $0 \leqslant r \leqslant 1$, where a small damping factor $\mathrm{e}^{\mathrm{i}\epsilon^* x}$ has been added to the forcing terms in the boundary condition (equation (2.11)) in order to ensure that the Fourier transform will exist. ϵ^* will be put equal to zero at the end of the analysis.

Equation (2.21) is the modified Bessel's equation of order one for $\hat{\phi}/r$, so that the solution that remains bounded at $r = 0$ is

$$\hat{\phi} = A(k)\,rI_1(kr). \tag{2.22}$$

It therefore follows from (2.13), (2.14), (2.17), (2.18) and (2.22) that

$$\hat{\theta}_- + \hat{\theta}_+ = -\mathrm{i}\left(\Omega - \frac{1-b}{1-\frac{1}{2}b}\,k\right)\left(1+\frac{kI_1'}{I_1}\right)\hat{\phi}_- \quad \text{at } r=1. \tag{2.23}$$

Eliminating $\hat{\zeta}_-$ and $\hat{\theta}_-$ between (2.19), (2.20) and (2.23) now yields

$$\chi(k)\,\hat{\phi}_- - \mathrm{i}\hat{\theta}_+ = \frac{\Omega}{2\pi(k-\mathrm{i}\epsilon^*)^2} - \frac{P_0}{2\pi(k-\mathrm{i}\epsilon^*)} - \frac{\mathrm{i}\zeta_x(0)}{2\pi\beta}, \tag{2.24}$$

for $\mathrm{Im}\,k = 0$, where

$$\chi(k) = \left(\Omega - k\frac{1-b}{1-\frac{1}{2}b}\right)\left[1+\frac{kI_1'(k)}{I_1(k)}\right] - \frac{2bk}{(1-\frac{1}{2}b)} - \frac{k^2(k^2-1)}{\beta\left[\Omega - \dfrac{1-b}{1-\frac{1}{2}b}\,k\right]}. \tag{2.25}$$

Equation (2.24) is a standard boundary-value problem for a sectionally analytic function. It follows from (2.18) and (2.22) that

$$A(k) = \frac{\hat{\phi}_-(k)}{I_1(k)}, \tag{2.26}$$

and that $A(k)$, and via (2.22) the complete solution, can be found once (2.24) is solved for $\hat{\phi}_-$. To this end we factorize χ in the form

$$\chi(k) = \frac{\chi_+(k)}{\chi_-(k)} \tag{2.27}$$

where the functions χ_+ and χ_- are analytic and non-zero in the upper and lower half-planes, respectively.

Since the kernel $\chi(k)$ is a meromorphic function of k the factorization (equation (2.27)) can be performed using the Weierstrass factorization theorem (Roos 1969 p. 174) to obtain

$$\chi_+(k) = \frac{\prod_{m=1}^{\infty}\left(1+\dfrac{k}{\zeta_m}\right)\mathrm{e}^{-k/\zeta_m}}{\prod_{n=1}^{\infty}\left(1+\dfrac{k}{\beta_n}\right)\mathrm{e}^{-k/\beta_n}}\,\mathrm{e}^{\tilde{\phi}(k)}, \tag{2.28}$$

and

$$\chi_-(k) = \frac{\left[\Omega - \dfrac{k(1-b)}{(1-\frac{1}{2}b)}\right]\left[\prod_{n=1}^{\infty}\left(1-\dfrac{k}{\beta_n}\right)\mathrm{e}^{k/\beta_n}\right]e^{\tilde{\phi}(k)}}{2\Omega^2\,\mathrm{e}^{k[(b-2)/\Omega(1-\frac{1}{2}b)]}\prod_{m=1}^{\infty}\left(1-\dfrac{k}{\xi_m}\right)\mathrm{e}^{k/\xi_m}}, \tag{2.29}$$

where β_n are the zeros of I_1/k in the upper half-plane, $-\zeta_m$ and ξ_m are the zeros of $\chi(k)\,I_1(k)/k$ in the lower and upper half-plane respectively, and $\tilde{\phi}(k)$ is an entire function which will be chosen so that χ_+ is algebraic at infinity.

Using a numerical search for the roots of (2.25) along with formal asymptotics we found that

$$\beta_n \sim \mathrm{i}\pi n + \tfrac{1}{4}\mathrm{i}\pi \quad \text{and} \quad \zeta_n \sim \mathrm{i}\pi n - \tfrac{7}{4}\mathrm{i}\pi,$$

as $n\to\infty$. Using these results in example (3.4) on p. 128 of Noble (1958) we find that we must take

$$\tilde{\phi}(k) = -k\sum_{n=1}^{\infty}\left(\frac{1}{\beta_n} - \frac{1}{\zeta_n}\right), \tag{2.30}$$

and that then

$$\chi_- \sim \left(\Omega - k\frac{1-b}{1-\frac{1}{2}b}\right)k^{-2} \quad \text{as } k\to\infty. \tag{2.31}$$

From (2.24) and (2.27) we can obtain

$$\frac{\hat{\phi}_-}{\chi_-}-\frac{\Omega}{2\pi\chi_+(i\epsilon^*)(k-i\epsilon^*)^2}+\frac{P_1}{2\pi(k-i\epsilon^*)\chi_+(i\epsilon^*)}$$
$$=\frac{i\hat{\theta}_+}{\chi_+}+\frac{\Omega}{2\pi(k-i\epsilon^*)^2}\left(\frac{1}{\chi_+(k)}-\frac{1}{\chi_+(i\epsilon^*)}\right)$$
$$-\frac{1}{2\pi(k-i\epsilon^*)}\left[\frac{P_0}{\chi_+(k)}-\frac{P_1}{\chi_+(i\epsilon^*)}\right]-\frac{i\zeta_x(0)}{2\pi\beta\chi_+(k)} \quad \text{for Im } k=0, \quad (2.32)$$

where we have introduced the new arbitrary constant

$$P_1 \equiv P_0+\frac{\Omega\chi_+'(i\epsilon^*)}{\chi_+(i\epsilon^*)}.$$

Since the left-/right-hand side of this equation is analytic in the lower-/upper-half k-plane it follows that (Noble 1958 p. 37)

$$\hat{\phi}_- = \frac{\chi_-}{2\pi\chi_+(i\epsilon^*)}\left[\frac{\Omega}{(k-i\epsilon^*)^2}-\frac{P_1}{(k-i\epsilon^*)}+E(k)\right], \quad (2.33)$$

where $E(k)$ is an arbitrary entire function of k, which by Liouville's theorem (Noble 1958 p. 6) must be a polynomial in k if $\hat{\phi}_-$ is to be algebraic at infinity. $\phi^{(1)}$ will have the minimum singularity at $x=0$ when A and consequently $\hat{\phi}_-$ has minimum singularity as $k\to\infty$ (Roos 1969 p. 150). This will occur if we put $P_1 = E = 0$. It now follows from (2.19), (2.31) and the inverse of (2.16) that our original assumption of $\zeta(0)=0$ is indeed satisfied, while (2.22), (2.26) and (2.33) and the definition of the Fourier transform imply that

$$\frac{\phi^{(1)}}{r} = \frac{\Omega}{2\pi}\oint_{-\infty}^{\infty}\frac{\chi_-(k)\,e^{ikx}}{\chi_+(0)\,k^2}\frac{I_1(kr)}{I_1(k)}\,dk, \quad (2.34)$$

where we have set $\epsilon^*=0$ with the understanding that the contour C passes below the pole at $k=0$.

In order to obtain the steady-state causal solution we must obtain the analytic continuation of (2.34) to $\text{Im}\,\Omega = 0$. For each mean velocity profile (equation (2.14)) there is a range of Weber numbers for which the flow is not absolutely unstable, and for each such Weber number there is a range of $\text{Re}\,\Omega$ for which the flow is convectively unstable. In this range one of the poles of χ_-, say at $k=\alpha$, moves from its position in the upper half k-plane, crosses the real axis, and ends up in the lower half-plane as $\text{Im}\,\Omega\to 0$. The analytic continuation of (2.34) is obtained by deforming the integration contour below this pole. The contour can then be moved back to the real axis by accounting for the residue at this pole as

$$\frac{\phi^{(1)}}{r} = \frac{\Omega}{2\pi}\oint_{-\infty}^{\infty}\frac{e^{ikx}\chi_-(k)}{k^2\chi_+(0)}\frac{I_1(kr)}{I_1(k)}\,dk-\frac{2i}{\alpha^2}C(\alpha)\,I_1(\alpha r)\,e^{i\alpha x}, \quad (2.35)$$

for $\text{Im}\,\Omega = 0$, where we have put

$$C(\alpha) = \frac{-\Omega\chi_+(\alpha)}{2\chi'(\alpha)\chi_+(0)\,I_1(\alpha)}. \quad (2.36)$$

In the remaining range of $\text{Re}\,\Omega$, i.e. the stable range, the pole moves onto the real axis. The result will still be given by (2.35) provided we interpret the integration

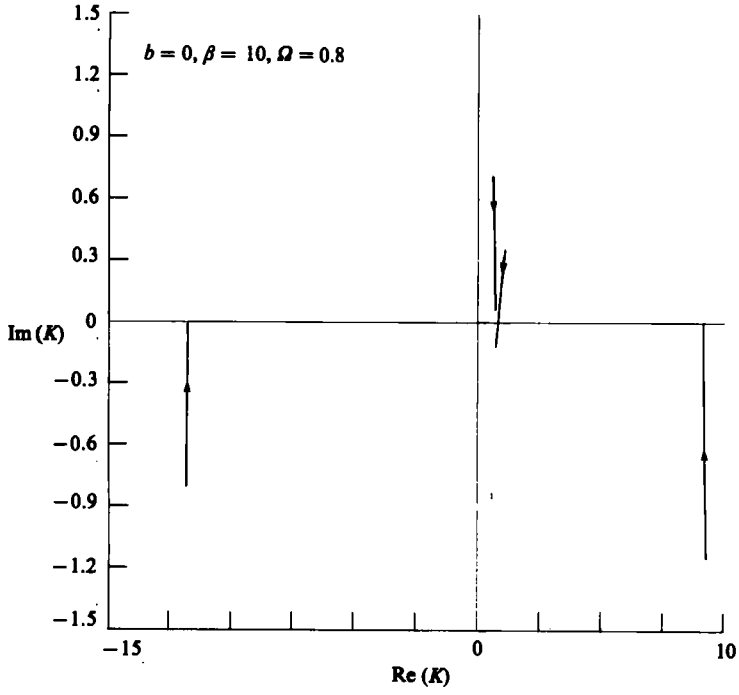

FIGURE 2. Movement of roots in complex plane, unstable case.

contour as lying above the pole at α. In the range of Weber numbers for which the flow is absolutely unstable the steady-state causal solution does not exist.

We can now obtain the complete solution for any physical quantity by substituting (2.35) into (2.9) and inserting the result into (2.4) or (2.2) via (2.3).

The integrands for the Fourier transforms of the velocities and pressure at $x = 0$, $r = 1$ all behave at least like k^{-1} as $k \to \infty$ so that (Roos 1969 p. 150) these quantities all remain finite at the edge i.e. the 'Kutta condition' is satisfied there. Other formal solutions can be obtained by allowing the polynomial E and the constant P_1 to be arbitrary, but their integrands would then be $O(1)$ or larger as $k \to \infty$ and they would consequently not exist as ordinary functions. If they are interpreted in a distributional sense they would have delta-function-type singularities at the edge (Lighthill 1958 p. 43).

3. The dispersion relation

In constructing the steady-state causal solution we had to consider the behaviour of one of the roots of $\chi(k)$ as $\operatorname{Im}\Omega \to 0$. However, it is of interest to consider the behaviour of all four roots of χ that can end up on, or cross, the real axis during this limiting process. This behaviour varies with the profile parameter, Strouhal number, and Weber number under consideration.

Figure 2 shows the loci of these roots for a case where the flow is unstable. When $\operatorname{Im}\Omega$ is large there are two roots each in the lower and upper half-planes. Those in the upper half-plane are poles of χ_- and consequently contribute to the solution (equation (2.34)) for $x > 0$. One of these (the one we called α in (2.35)) starts out in the upper half-plane, crosses the real axis and moves into lower half-plane as $\operatorname{Im}\Omega \to 0$. Figure 3 shows the loci of these roots for the same profile and Weber number but

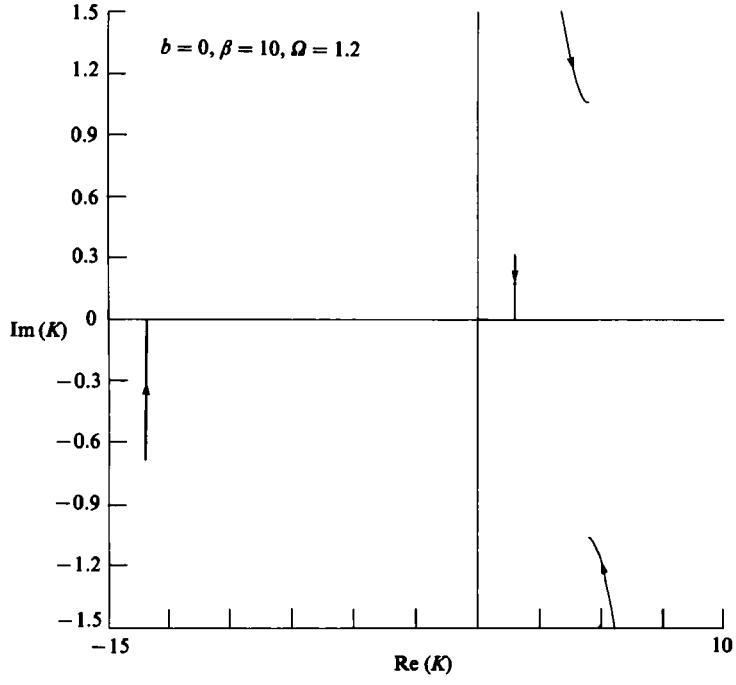

FIGURE 3. Movement of roots in complex plane, stable case.

at a higher Strouhal number. There is again one pair of roots in each half-plane for large Im Ω but the root α now moves onto the real axis when Im $\Omega = 0$ and therefore, as was indicated in the previous section, represents a neutral wave. The loci of the roots for a third set of parameters are shown in figure 4. The flow is again stable but α now crosses over into the lower half-plane before turning around to end up back on the real axis when Im $\Omega = 0$. The group velocity $\mathrm{d}\Omega/\mathrm{d}k$ is negative for the resulting neutral wave even though it appears downstream of the duct exit and consequently represents a downstream propagating wave. This phenomenon was discussed by Briggs (1964 pp. 33–34) who points out that the group velocity does not always give the correct direction of propagation for neutral waves in an unstable medium.

Figure 5 shows the behaviour of the four roots of interest as Re Ω varies, with Im Ω fixed at a small positive value for the sake of clarity.† The velocity profile and Weber number are the same as in figures 2 and 3. The arrows point in the direction of increasing Re Ω. There are two complex conjugate roots (denoted by ① and ②) below a certain Strouhal number (the cutoff Strouhal number referred to in §1). One of these (root ②) is associated with the instability wave. The roots merge at the cutoff Strouhal number (point A in figure 5) to form a double root or saddle point of the dispersion relation at real values of k and Ω. This behaviour was referred to as a 'direct resonance' by Akylas & Benney (1980) who showed that it can increase the importance of the nonlinear effects. Here the two roots correspond to waves travelling in the same (downstream) direction (see figure 2), since they both move into the upper half-plane as Im Ω becomes large. As Re Ω increases beyond the cutoff frequency the roots separate but both move along the real axis until roots ① and ④ merge and form a double root or 'direct resonance' (point B). The two roots now correspond to waves travelling in opposite

† For example it allows us to keep track of the roots after they merge.

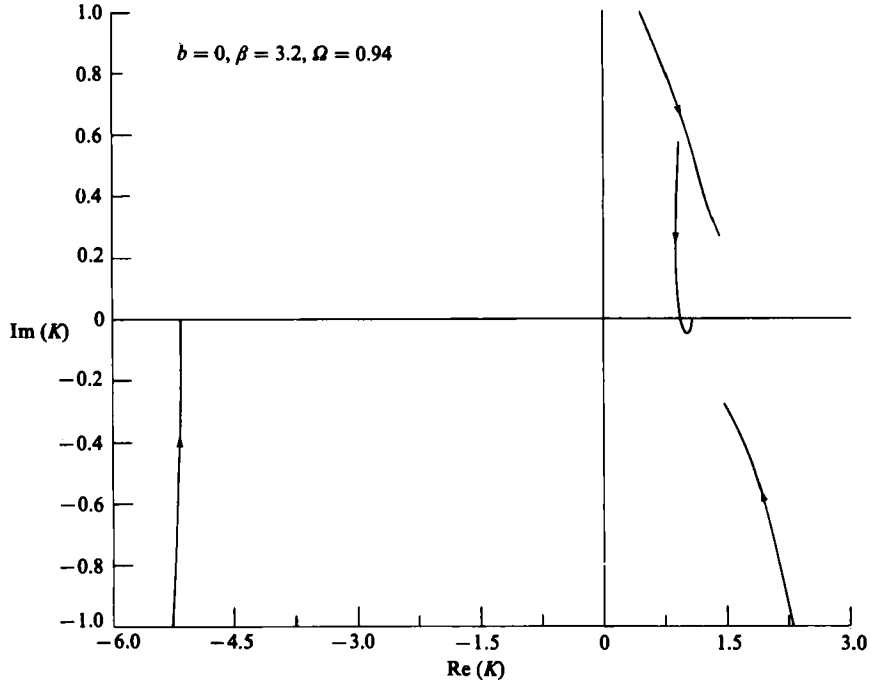

FIGURE 4. Movement of roots in complex plane, stable case.

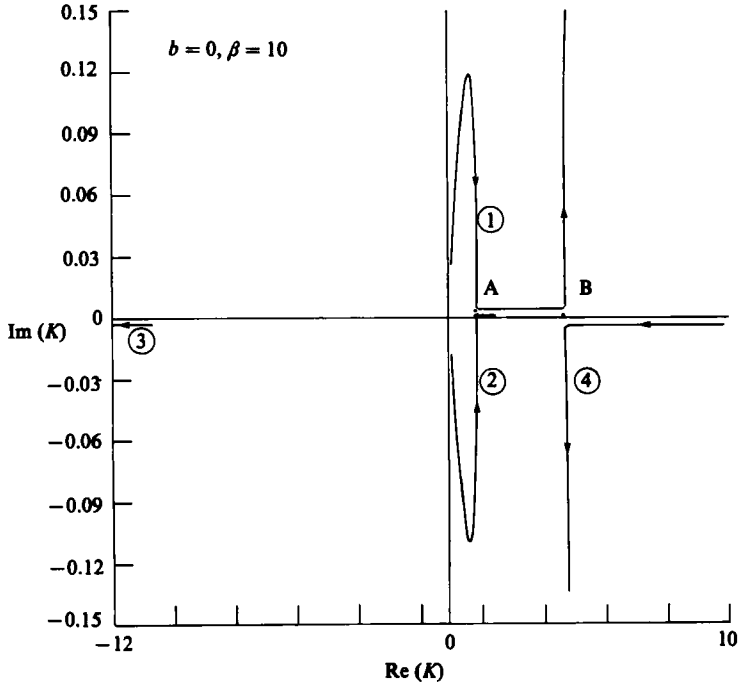

FIGURE 5. Movement of roots in complex plane as Re Ω increases.

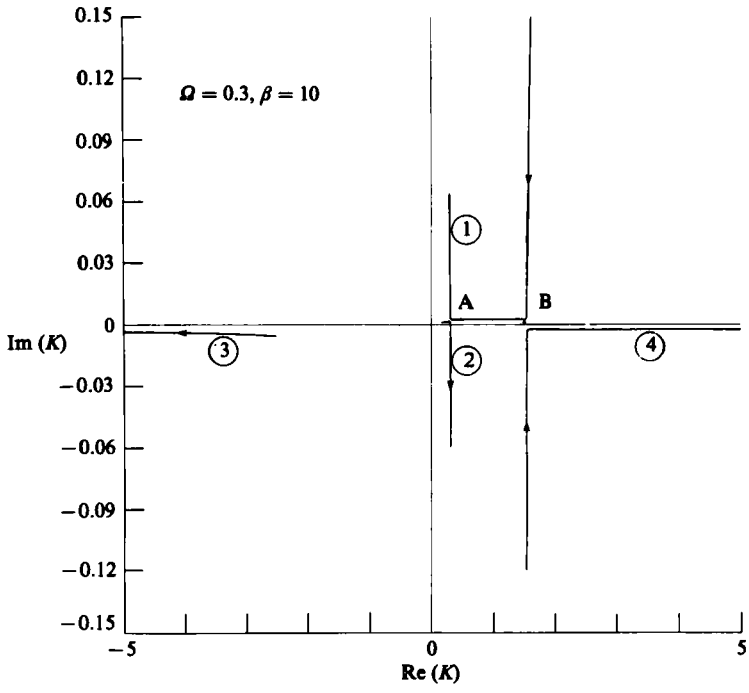

FIGURE 6. Movement of roots in complex plane as b goes from 1 to 0.

directions. As $\mathrm{Re}\,\Omega$ is further increased the roots break away from the real axis to form a new complex conjugate pair. The one in the lower half-plane does not, however, represent a spatially amplifying wave in the causal solution because (as shown in figure 3) it does not cross the real axis as $\mathrm{Im}\,\Omega \to 0$ with $\mathrm{Re}\,\Omega$ fixed.

For reasons given in §1, we are interested in the behaviour of the roots as the velocity profile relaxes toward the plug-flow profile. The movement of the roots with the profile shape parameter b is shown in figures 6 and 7 for two different Strouhal and Weber numbers. The arrows point in the direction of decreasing b.

Root ② again corresponds to the instability wave and the movement of this root in the direction of the arrow corresponds to the evolution of that wave as the mean profile relaxes. The wave is neutral for the Hagen–Poiseuille profile ($b = 1$) but turns into a spatially growing wave whose growth rate continues to increase as the profile relaxes toward the plug-flow profile (i.e. as $b \to 0$). The wave exhibits growth for larger values of b (i.e. profiles closer to Hagen–Poiseuille) at lower values of the Strouhal number. Note that the wave must pass through the neutral point A, where the dispersion relation has a double root (or saddle point), before it can exhibit growth. Root ①, which initially corresponds to a decaying wave, passes through the saddle point B before it turns into a neutral wave.

As indicated above, the time harmonic causal solution only exists when (2.34) can be analytically continued by deforming its integration contour around any poles that cross the real axis as $\mathrm{Im}\,\Omega \to 0$. This will not be possible if two roots from opposite half-planes merge to form a double root in the lower half k-plane for some $\mathrm{Im}\,\Omega > 0$, because the contour will then be pinched between these roots. The steady-state causal solution will then not exist and the flow is said to be 'absolutely unstable' (Briggs 1964 p. 20). This occurs for Weber numbers below a certain critical value which

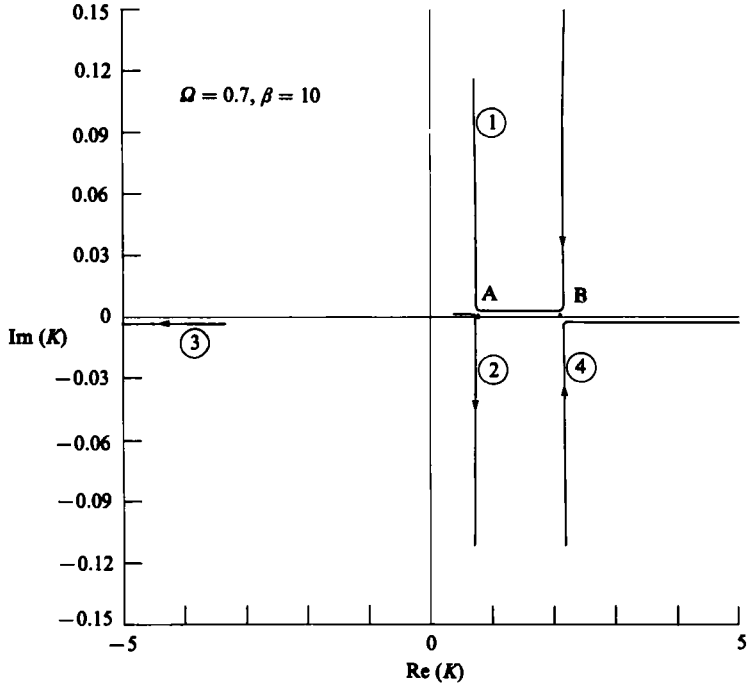

FIGURE 7. Movement of roots in complex plane as b goes from 1 to 0.

decreases markedly as the shape parameter $b \to 1$. The double root now corresponds to two waves travelling in opposite directions.

As far as we know, the existence of absolute instability for capillary (i.e. Rayleigh) waves has not been previously noted – even for the plug flow profile studied by Rayleigh (1878) and Keller *et al.* (1973).

Figure 8 shows the loci of the two relevant roots as $\mathrm{Im}\,\Omega$ varies for a number of values of $\mathrm{Re}\,\Omega$. It can be seen that for the particular case shown ($b = 0$ and $\beta = 1$), the roots merge for Ω in the upper half-plane with $0.74 < \mathrm{Re}\,\Omega < 0.78$.

As the Weber number is increased (with the profile shape fixed) this double root moves closer to the real Ω-axis. We refer to the minimum value of β for which this double root occurs at $\mathrm{Im}\,\Omega = 0$ for any given profile shape as the critical Weber number β_c. The flow is then convectively unstable for $\beta > \beta_c$.

As in the 'direct resonance' discussed above, the double root of the dispersion relation occurs at real values of Ω when $\beta = \beta_c$ and can consequently have a profound effect on the steady state, i.e. time harmonic, weakly nonlinear or weakly non-parallel solution for the capillary waves. However, it now occurs at a complex value of k and results from the coalescence of roots associated with waves travelling in *opposite directions*. It is therefore more like the resonance at point B in figures 5–7 than at the neutral point A. Figure 9 is a plot of the critical Weber number as a function of b.

The wavenumber and growth rate of the instability wave are given by the real and imaginary parts, respectively, of the root α of χ. They are plotted as a function of Ω for various Weber numbers and profile shape parameters in figures 10–17. Figures 10–13 show that the maximum growth rate decreases and shifts to lower Strouhal numbers with increasing Weber number for a given profile shape. The plug-flow profile

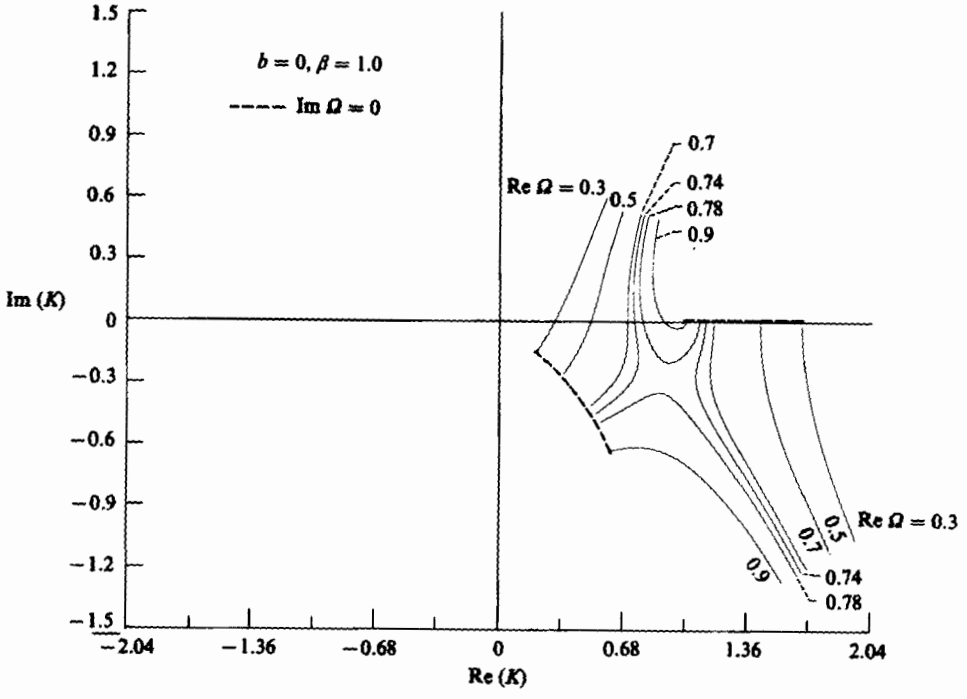

FIGURE 8. Movement of roots in complex plane, absolute instability.

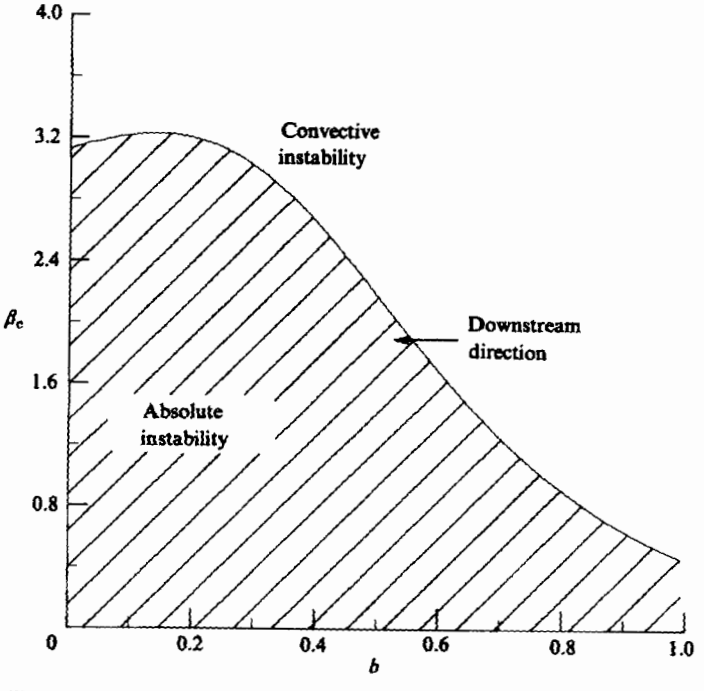

FIGURE 9. Critical Weber number as a function of profile parameter.

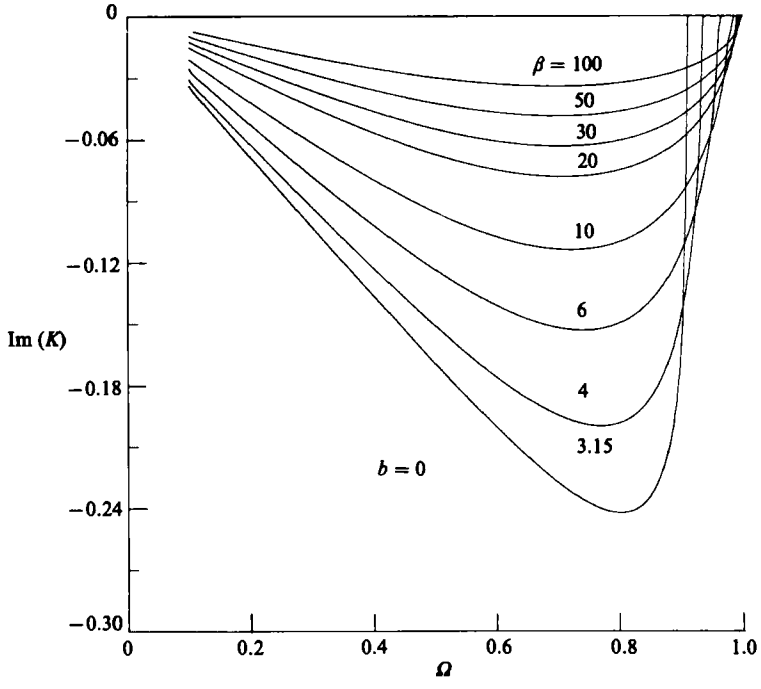

FIGURE 10. Growth rates for instability waves.

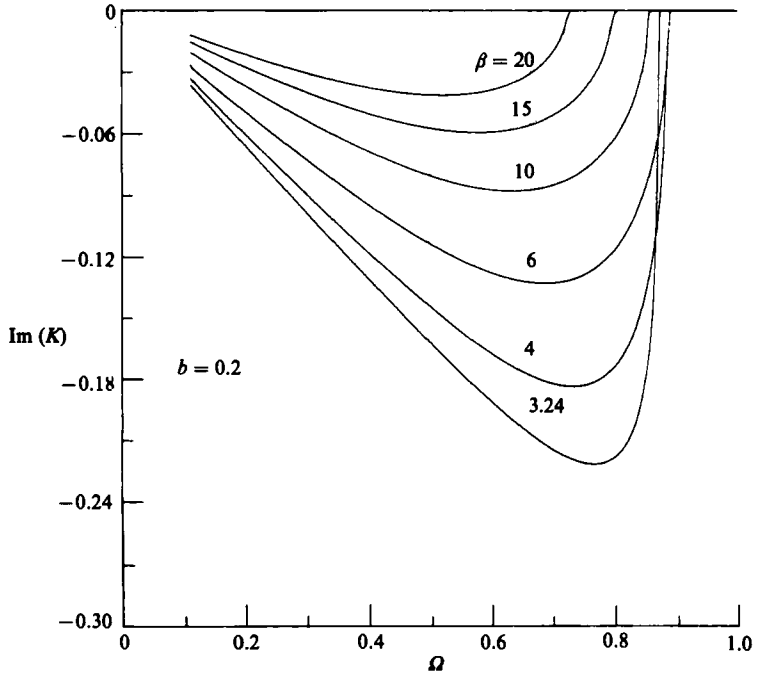

FIGURE 11. Growth rates for instability waves.

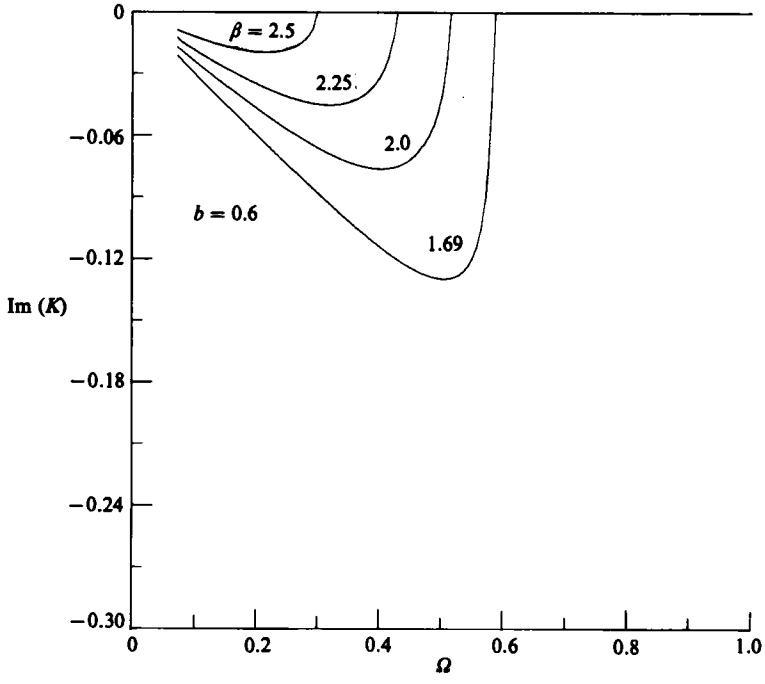

FIGURE 12. Growth rates for instability waves.

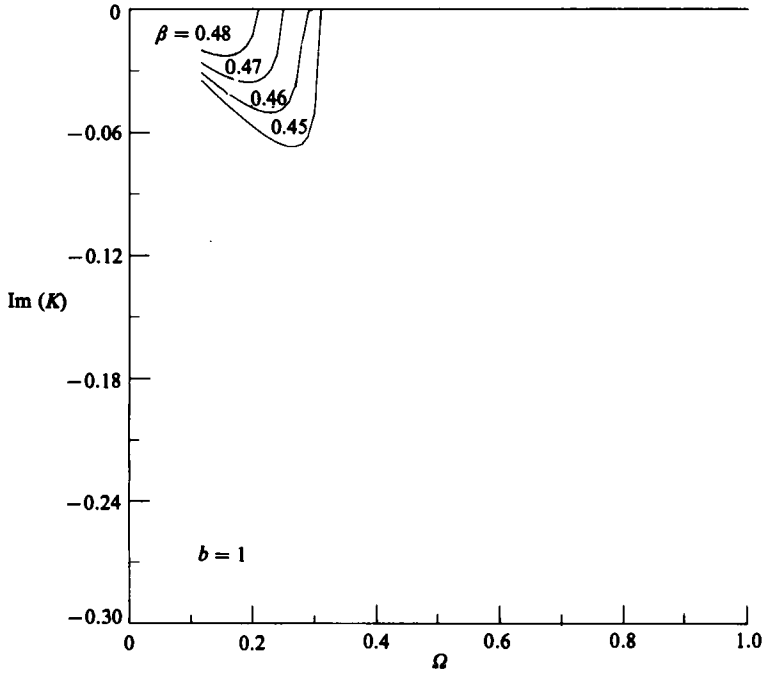

FIGURE 13. Growth rates for instability waves.

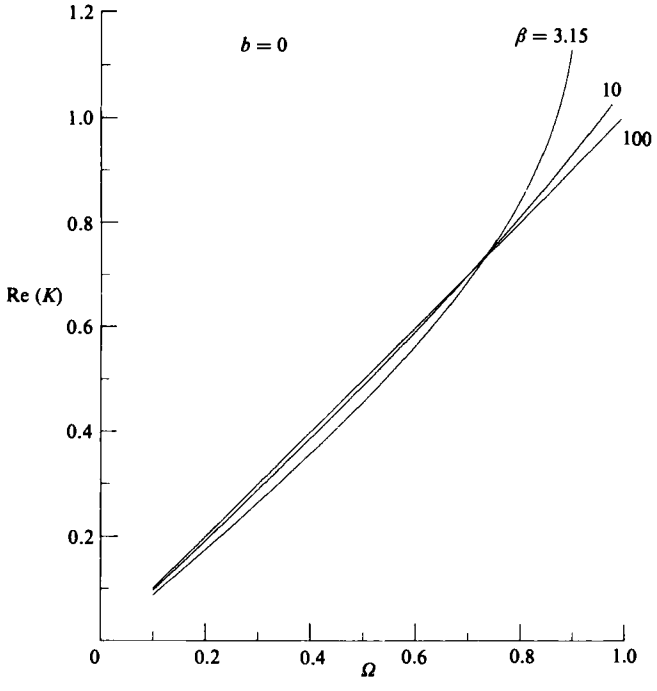

FIGURE 14. Wavenumbers for instability waves.

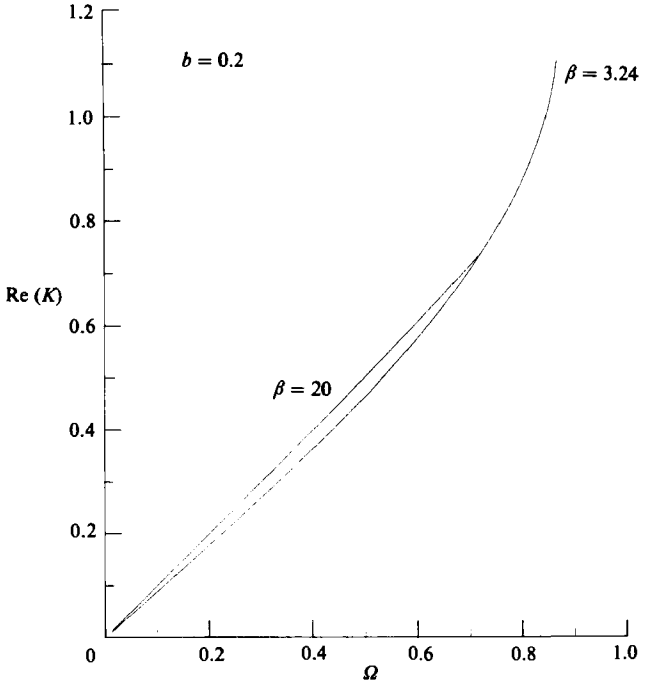

FIGURE 15. Wavenumbers for instability waves.

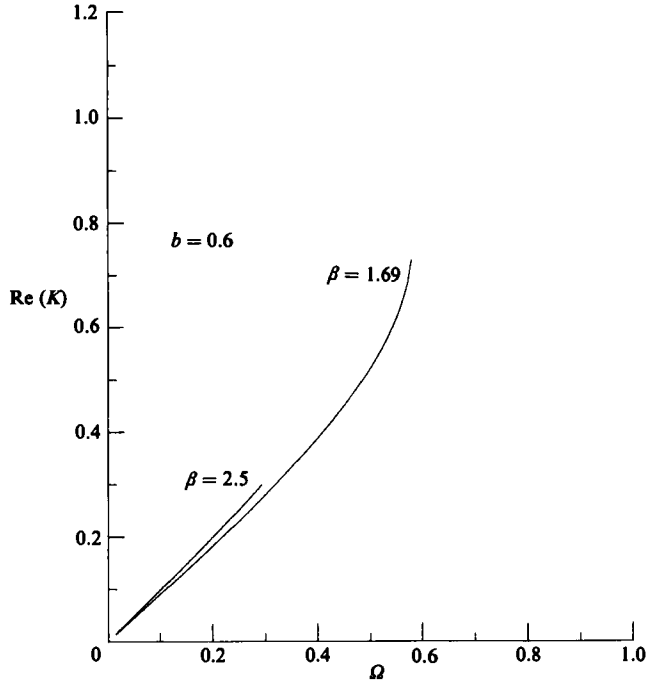

FIGURE 16. Wavenumbers for instability waves.

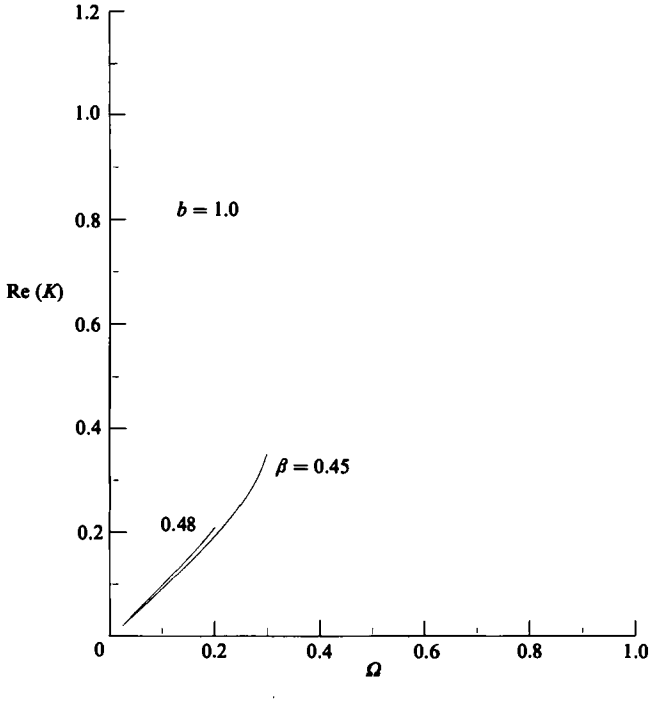

FIGURE 17. Wavenumbers for instability waves.

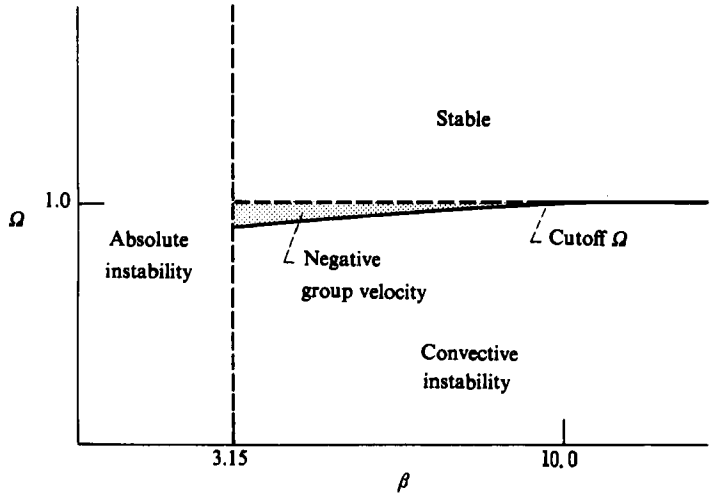

FIGURE 18. The stability regimes in the (Ω, β)-plane for $b = 0$.

($b = 0$) is clearly much more unstable than the Hagen–Poiseuille profile in terms of both growth rates and range of unstable frequencies. The unstable Weber numbers are also very small in the latter case. There is virtually no growth for realistic values of β but, as explained in §1, the neutral disturbances can ultimately turn into amplifying waves as the profile relaxes toward a plug flow.

Figures 14–17 show that the wavelengths of the instability waves decrease with increasing Strouhal number, while being relatively independent of Weber number and mean profile shape.

Figure 18 summarizes the stability regimes in the (Ω, β)-plane for the plug-flow profile. The critical Weber number for this profile ($\beta_c = 3.15$) divides the plane into a region of absolute instability ($\beta_c < 3.15$) and a region of convective instability ($\beta_c > 3.15$). The cutoff Strouhal number separates the stable and unstable regimes for $\beta > \beta_c$. Also shown is the area (within the stable regime) where the neutral waves have negative group velocity. It does not persist beyond Weber numbers of about 10, where the cutoff Strouhal number is equal to unity independently of the Weber number.

4. Discussion

The constant C in (2.36) is equal to the streamwise velocity of the instability wave (or of the neutral disturbance that turns into the instability wave) at the origin $(x, r) = (0, 0)$ normalized by the imposed streamwise velocity fluctuation at upstream infinity. We refer to it as the 'coupling coefficient' since it measures the efficiency of the instability wave-generation process. Equation (2.36) was used to obtain numerical values for C.

α and the ζ_m were obtained using the Newton–Raphson method to find the zeros of $\chi(k) I_1(k)$ for various values of the Strouhal and Weber numbers. $\chi_+(\alpha)$ was then calculated from (2.28) and $\chi'(\alpha)$ from the derivative of (2.25). These results were combined in (2.36) to calculate C at a given Ω and β.

The absolute value of this quantity is plotted for a Hagen–Poiseuille profile in figure 19 over the range of unstable Weber and Strouhal numbers and over the stable range

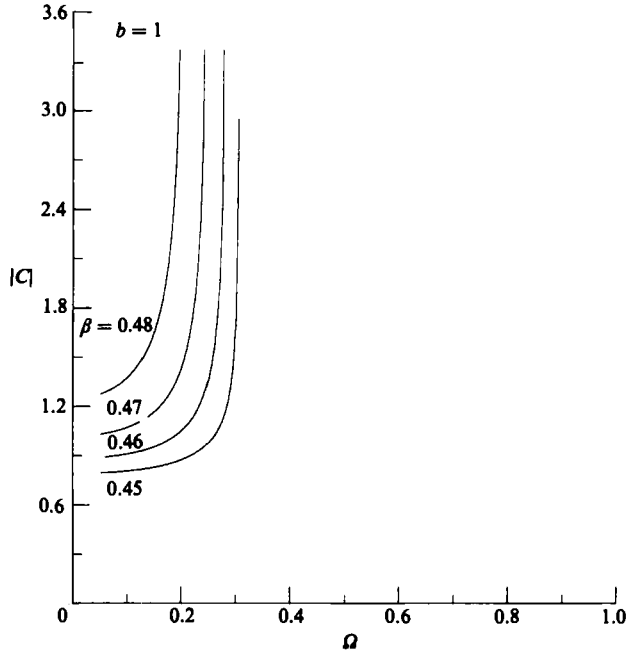

FIGURE 19. Coupling coefficient as a function of Ω for a number of β-unstable range.

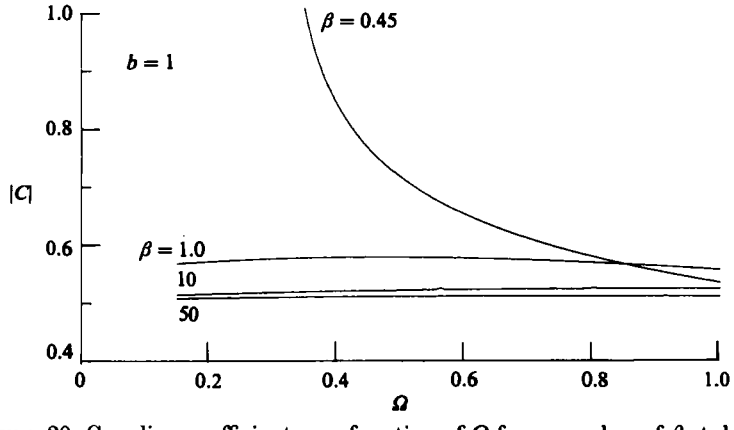

FIGURE 20. Coupling coefficient as a function of Ω for a number of β-stable range.

in figure 20. Figure 21 is a plot of $|C|$ in the unstable range for the plug-flow profile. It is worth noting that χ_- has a second-order pole at the cutoff Strouhal number, which corresponds to the double root 'direct resonance' at this point that was discussed in §3. $|C|$ is relatively independent of Ω and β for β greater than about one, except in the immediate vicinity of the cutoff frequency where it becomes quite large. As the Weber number increases, $|C|$ approaches a value of about 0.5 for the Hagen–Poiseuille profile and 0.25 for the plug profile.

Koch (1985) recently suggested that vortex shedding from a blunt body may be related to the occurrence of a double root of the dispersion relation associated with an absolute instability of an appropriate family of wake profiles that describe the mean wake as it evolves downstream. As explained above, the relevant double root

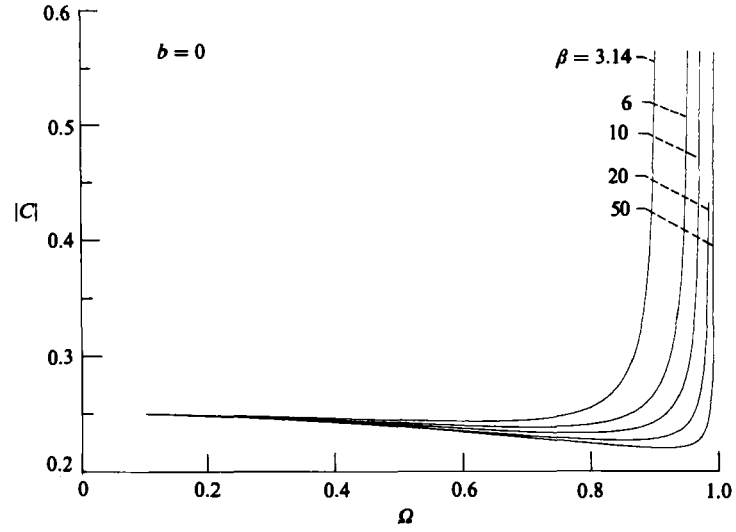

FIGURE 21. Coupling coefficient as a function of Ω for a number of β-unstable range.

occurs at a real frequency and is associated with the profile at the 'resonance point' that forms the boundary between the region of absolute instability and the region of convective instability.

While Koch (1985) found that the corresponding frequencies are in good agreement with experimentally observed vortex-shedding frequencies, his model suffers from the conceptual difficulty that the flow is absolutely unstable between the trailing edge and the 'resonance point', implying that the intermediate profiles in his analysis would not occur in practice.

But the situation is just the reverse in the present case, i.e. the flow is convectively unstable upstream of the 'resonance point' and absolutely unstable downstream (provided, of course, that the Weber number is in the range where the plug-flow profile is absolutely unstable and the Hagen–Poiseuille profile is not). Then, as the mean flow relaxes from the latter to the former, a point is reached where the local profile just becomes absolutely unstable and the dispersion relation has a double root or saddle point at real Ω.

We might expect, in view of Koch's (1985) success in predicting vortex-shedding frequencies, that the double root in the present flow will be associated with some natural droplet formation process, but this needs to be studied further. Notice, however, that the critical Weber number β_c is always rather small, so that it might be difficult to achieve the relevant conditions in the laboratory.

The downstream propagating wave will be neutral on the Hagen–Poiseuille profile that exists at the nozzle exit for Weber numbers above the maximum critical Weber number (i.e. for Weber numbers where the flow is everywhere convectively unstable). There will then be a downstream position where the Strouhal number of the disturbance coincides with the 'cutoff' Strouhal number for the local profile and, as pointed out in §3, the flow will then exhibit a 'direct resonance' associated with the coalescence of two waves travelling in the same direction.

Unlike the previous case, the entire flow is now convectively unstable and the Weber number can be fairly large so that, on the face of it, one might expect these conditions to be achievable in the laboratory. But we expect that the relevant double root only occurs because the idealized profile considered herein has no critical layer

and that the branch cut associated with this critical layer would eliminate the need for one of the roots that comprises that particular double root of the dispersion relation (Lin 1955 pp. 125–135). The alteration in the nonlinear behaviour that would have resulted from the 'direct resonance' will, for a more realistic profile, manifest itself as a nonlinear critical layer phenomenon (Benney & Bergeron 1969).

The numerical computations show that the coupling between the imposed disturbance and the downstream travelling wave triggered at the trailing edge is more efficient for the Hagen–Poiseuille profile (by a factor of about 2 for large β). It might therefore seem advantageous to make the nozzle long enough to achieve fully developed flow when attempting to acoustically excite the jet. But very large coupling coefficients can be achieved for any exit profile if the jet is excited at the cutoff frequency, and the effects of the smaller coupling at other frequencies will, in any case, always be overcome by the much larger growth rates that occur on the flatter profiles. Figures 10 and 13 show that the maximum growth rate for the plug-flow profile is nearly four times larger than that for the Hagen–Poiseuille profile and that the unstable Strouhal number range is about three times larger.

The relaxation of the mean velocity profile was modelled using (2.14) and allowing the parameter b to vary between 1 and 0. To obtain some idea of the lengthscale over which the profile relaxation occurs we note that Scriven & Pigford (1959) made measurements of liquid-jet diameters and estimated the downstream distance at which the plug-flow profile was reached. They found that the velocity profiles became flat at about 60 nozzle radii downstream (for Reynolds numbers of around 250). Since the instability waves have wavelengths of the order of the radius this shows that the profile relaxation takes place over many wavelengths and consequently that the slowly varying approximation is valid.

Scriven & Pigford's (1959) results also suggest that $b \sim x^{-\frac{1}{2}}$ as $x \to \infty$. Hence b goes to zero like the inverse square root of the streamwise coordinate in the final approach to the plug-flow profile.

REFERENCES

Akylas, T. R. & Benney, D. J. 1980 Direct resonance in non-linear wave systems. *Stud. Appl. Maths* **63**, 209–226.

Benney, D. J. & Bergeron, R. F. 1969 A new class of non-linear waves in parallel flows. *Stud. Appl. Maths* **48**, 181–204.

Brazier-Smith, P. R. & Scott, J. F. 1984 Stability of fluid flow in the presence of a compliant surface. *Wave Motion* **6**, 547–560.

Briggs, R. J. 1964 *Electron Stream Interaction with Plasmas*. MIT Press.

Cargill, A. M. 1979 Low frequency sound radiation due to the interaction of unsteady flows with a jet pipe. In *Mechanics of Sound Generation in Flows*, pp. 19–25. Springer.

Crighton, D. G. & Leppington, F. G. 1974 Radiation properties of the semi-infinite vortex sheet. *J. Fluid Mech.* **64**, 393–414.

Drazin, P. G. & Reid, W. H. 1981 *Hydrodynamic Stability*. Cambridge University Press.

Keller, J. B., Rubinow, S. I. & Tu, Y. O. 1973 Spatial instability of a jet. *Phys. Fluids* **16**, 2052–2055.

Koch, W. 1985 Local instability characteristics and frequency determination of self-excited wake flows. *J. Sound Vib.* **99**, 53–83.

Lighthill, M. J. 1958 *An Introduction to Fourier Analysis and Generalised Functions*. Cambridge University Press.

Lin, C. C. 1955 *The Theory of Hydrodynamic Stability*. Cambridge University Press.

MORKOVIN, M. V. 1969 Critical evaluation of transition from laminar to turbulent shear layer with emphasis on hypersonically travelling bodies. *Air Force Flight Dynamics Lab. Rep.* AFFDL-TR-68-149. (AD-686178).

MUNT, R. M. 1977 The interaction of sound with a subsonic jet issuing from a semi-infinite circular pipe. *J. Fluid Mech.* **83**, 609–690.

NOBLE, B. 1958 *Methods Based on the Wiener–Hopf Technique for the Solution of Partial Differential Equations*. Pergamon.

RAYLEIGH, LORD 1878 On the instability of jets. *Proc. Lond. Math. Soc.* **10**, 4–13.

RIENSTRA, S. W. 1981 On the acoustical implications of vortex shedding from an exhaust pipe. *J. Engng Ind.* **103**, 378–384.

ROOS, B. W. 1969 *Analytic Functions and Distributions in Physics and Engineering*. Wiley.

SCRIVEN, L. E. & PIGFORD, R. L.. 1959 Fluid dynamics and diffusion calculation for laminar liquid jets. *AIChE J.* **5**, 397–402.